Elsevier Editorial System(tm) for Ceramics International

Manuscript Draft

Manuscript Number: CERI-D-15-04553R1

Title: Metal-supported SOFC with an aerosol deposited in-situ LSM and 8YSZ composite cathode

Article Type: Full Length Article

Keywords: metal-supported solid oxide fuel cells (MS-SOFCs), aerosol deposition process (ADP), cathode, sintering process, electrochemical property

Corresponding Author: Prof. Jung Hyun Kim, Ph.D

Corresponding Author's Institution: Hanbat National University

First Author: Seung-Wook Baek, Ph.D

Order of Authors: Seung-Wook Baek, Ph.D; Jihoon Jeong, Ph.D candidate; Harald Schlegl, Ph.D; Azad Abul K., Ph.D ; Dae Soo Park, M.S. candidate; Un Bong Baek, Ph.D; Jung Hyun Kim, Ph.D

Abstract: This study reports the micro-structural and electrochemical properties of metal-supported solid oxide fuel cells (MS-SOFCs) with an La0.8Sr0.2MnO3-d (LSM) /8 mol % yttria-stabilized zirconia (8YSZ) composite cathode, fabricated at room temperature using the aerosol deposition process (ADP). The composite cathode fabricated with the ADP technique shows uniform distribution of components and pores and the interface between the cathode and the electrolyte displays excellent joining properties. The area specific resistance (ASR) of the ADP-LSM/8YSZ sample is approximately 1.50 Ω·cm2 at 800 oC, so this sample shows a significantly lower ASR value than the values usually reported for samples fabricated by the in-situ treatment method for MS-SOFCs. The power density of the cells with the ADP-LSM/8YSZ cathode coated on MS-SOFCs shows a maximum value of 0.38 mW·cm-2 at 800 °C and stable performance in the severe thermal durability test. Therefore, these research results can broaden the opportunities for adoption of the ADP coating processes to fabricate cathode materials in MS-SOFCs.

Detailed Responses to Reviewers

Ref. No.: CERI-D-15-04553

Title: Metal-supported SOFC with an aerosol deposited in-situ LSM and 8YSZ composite cathode

Dear editor and reviewers of Ceramics International:

I am Jung Hyun Kim, a corresponding author of the manuscript "Metal-supported SOFC with an aerosol deposited in-situ LSM and 8YSZ composite cathode." Above all, I would like to thank you for your comments. Revised expressions or explanations from reviewers were written with **blue color** and minor corrections from professional proofreader were written with **red color** in the modified manuscript and "Detailed Response to Reviewers" file. The revisions with respect to the comments from each reviewer are as follows:

Reviewer #1:

1) Figure 1 - Are there possibly secondary peaks in the XRD pattern for the ADP sample at approximately 28º and 54º ?

→ Minor XRD peaks at approximately 28º and 54º can be observed in Fig. 1(a). However, they were not found in Fig. 1(b).

When comparing the XRD patterns measured at 28º and 54º, shown in Fig. 1(a) of this manuscript, with patterns found in the literature for $La_{0.8}Sr_{0.2}MnO_{3-d}$ ([20] D. Grossin , J.G. Noudem, Synthesis of fine $La_{0.8}Sr_{0.2}MnO_3$ powder by different ways, Solid State Sciences 6 (2004) 939-944, [21] V. S. Reddy Channu, R. Holze, E. H. Walker, Synthesis and characterization of $La_{0.8}Sr_{0.2}MnO_{3-\delta}$ nanostructures for solid oxide fuel cells, New Journal of Glass and Ceramics, 3 (2013) 29-33) and 8YSZ ([23] C.W. Kuoa, Y. H. Shena, I. M. Hung, S.

B. Wenc, H. E. Lee, M. C. Wang, Effect of Y_2O_3 addition on the crystal growth and sintering behavior of YSZ nanopowders prepared by a sol-gel process, Journal of Alloys and Compounds 472 (2009) 186-193), the peak at approximately 28º, shown in Fig. 1(a), came from the background noise effect; the peak in the vicinity of 54º, shown in Fig. 1(a), originated from $La_{0.8}Sr_{0.2}MnO_{3-d}$. Therefore, an open circle (o) on the 54º peak was also added in Fig. 1(a) of the modified manuscript.

In addition, the peak in the vicinity of 78º was also assigned to $La_{0.8}Sr_{0.2}MnO_{3-d}$ and an open circle was added to Fig. 1(a).

Literature references [20, 21, 22] that show LSM and 8YSZ single phases were also added in blue color in the modified manuscript.

2) Decomposition of PVdF is not the only reason for the generation of porosity. If possible, could you explain microstructural changed in the point of particle sintering effect?

→ The porous structures shown in Figs. 4(a) and (b) were caused by the decomposition of PVdF organic material.

When increasing the heat treatment temperature from 800 ^oC to 1100^oC, the sintering effect of the composite cathodes comprised of LSM and 8YSZ was also measured; significantly, the relatively dense structure shown in Fig. 4(b), compared to that shown in Fig. 4(a), is believed to be caused by the sintering effect at high temperature.

Therefore, the sentence “In addition, when increasing the heat treatment temperature from 800 ^oC to 1100 ^oC, the sintering effect of the composite cathodes comprised of LSM and 8YSZ was also measured; significantly, the relatively dense structure shown in Fig. 4(b), compared to that shown in Fig. 4(a), is believed to be caused by the sintering effect at high temperature.” was added in blue color in the modified manuscript.

3) When discussing thermal cycle (Fig. 8), the size of the cell or stack should be described because they significantly affect on the characteristics.

→A button cell was used to measure the current (I) - voltage (V) - power density (P), long term stability and thermal cycling stability of the ADP-LSM/8YSZ coated MS-SOFC. The final cathode surface area and thickness were about 1 cm^2 and 12 μm. The thickness of the anode-supported ceramic cell without cathode and metal support was 1 mm.

In addition, the sentence describing the size of the cell "The final cathode surface area and thickness were about 1 cm^2 and 12 μm. The thickness of anode-supported ceramic cell without cathode and metal support was 1 mm." was also added in section 2.3 Fabrication process of MS-SOFC of experimental section in blue color.

Other minor modifications in the revised manuscript

1) In abstract section, minor modifications were written with red color.

2) In introduction section, minor modifications were written with red color.

3) In experimental section, minor modifications were written with red color.

4) In results and discussion section, minor modifications were written with red color.

5) On page 7, the phrase of "XRD patterns can be assigned to either YSZ or a LSM" was changed to "XRD patterns can be assigned to either an LSM or to an 8YSZ"

6) Reference numbers of [20], [21], [22], [23], [24] in the previous manuscript were changed to [23], [24], [25], [26], [27] in the revised manuscript.

7) In conclusions section, minor modifications were written with red color.

8) In acknowledgements section, minor modifications were written with red color.

9) In references section, minor modifications were written with red color.

10) In figure captions section, minor modifications were written with red color.

11) The legend color of Fig. 6 was changed to black and the summarized fitting ASR values

were changed to a black dash line.

Metal-supported SOFC with an aerosol deposited *in-situ* LSM and 8YSZ composite cathode

Seung-Wook Baek [a], Jihoon Jeong [b], Harald Schlegl [c], Abul K. Azad [d], Dae Soo Park [e]

Un Bong Baek [a,*], Jung Hyun Kim [e,*]

[a] Center for Energy Materials Metrology, Division of Industrial Metrology, Korea Research Institute of Standards and Science (KRISS), 267 Gajeong-Ro, Yuseong-Gu, Daejeon 305-340, Republic of Korea

[b] Department of Mechanical Engineering, The University of Texas at Austin, Austin, TX 78712, USA

[c] Engineering Department, Lancaster University, Bailrigg, Lancaster LA1 4YW, United Kingdom

[d] Faculty of Integrated Technologies, University Brunei Darussalam, Jalan Tunku Link, Gadong, BE1410, Brunei Darussalam

[e] Department of Advanced Materials Science and Engineering, Hanbat National University, 125, Dongseo-Daero, Yusung-Gu, Daejeon, 305-719, Republic of Korea

Corresponding authors:*

Jung Hyun Kim: jhkim2011@hanbat.ac.kr, jhkim1870@gmail.com Tel: +82-42-821-1239, Fax: +82-42-821-1592, Department of Advanced Materials Science and Engineering, Hanbat National University, 125, Dongseo-Daero, Yusung-Gu, Daejeon, 305-719, Republic of Korea

Un Bong Baek: ubbaek@kriss.re.kr, Tel: +82-42-868-5384, Fax: +82-42-868-5635, Center for Energy Materials Metrology, Division of Industrial Metrology, Korea Research Institute of Standards and Science (KRISS), 267 Gajeong-Ro, Yuseong-Gu, Daejeon 305-340, Republic of Korea

Abstract

This study reports the micro-structural and electrochemical properties of metal-supported solid oxide fuel cells (MS-SOFCs) with an $La_{0.8}Sr_{0.2}MnO_{3-d}$ (LSM) /8 mol % yttria-stabilized zirconia (8YSZ) composite cathode, fabricated at room temperature using the aerosol deposition process (ADP). The composite cathode fabricated with the ADP technique shows uniform distribution of components and pores and the interface between the cathode and the electrolyte displays excellent joining properties. The area specific resistance (ASR) of the ADP-LSM/8YSZ sample is approximately 1.50 $\Omega \cdot cm^2$ at 800 ^oC, so this sample shows a significantly lower ASR value than the values usually reported for samples fabricated by the *in-situ* treatment method for MS-SOFCs. The power density of the cells with the ADP-LSM/8YSZ cathode coated on MS-SOFCs shows a maximum value of 0.38 $mW \cdot cm^{-2}$ at 800 °C and stable performance in the severe thermal durability test. Therefore, these research results can broaden the opportunities for adoption of the ADP coating processes to fabricate cathode materials in MS-SOFCs.

Keywords: metal-supported solid oxide fuel cells (MS-SOFCs), aerosol deposition process (ADP), cathode, sintering process, electrochemical property

1. Introduction

Metal-supported solid oxide fuel cells (MS-SOFCs) have been investigated as high-potential energy devices because they exhibit high mechanical strength, excellent sealing efficiency, and improved thermal resistance, as well as having a quick start up performance when compared to that of conventional SOFCs [1-6]. In spite of the many advantages of MS-SOFCs, there are many limitations in the fabrication process caused by the direct contact between the metal and ceramic components [7-10]. For example, sintering the cathode material under oxidizing conditions is impossible if the cathode is attached to the substrate, and combined with a metal part, because this combination has to be fabricated under reducing conditions. The use of high temperature sintering is also confined by the oxidation of the metal substrate used for the interconnector, the oxidation of the Ni-Cr-Fe material used for the cohesive layer and the oxidation of the anode substrate comprised of NiO-8YSZ [7, 11].

To solve the problems mentioned above, many studies have reported on relevant topics like atmospheric plasma spray coating [12], pulsed laser deposition (PLD) [2], wet ceramic processes [2], high temperature sintering in a reducing condition [13] and vacuum plasma spray processing [14].

Recently, an aerosol deposition process (ADP) method to form ceramic films has been developed; because ADP can form either a thick and dense ceramic coating layer or induce the growth of the deposited phase in the bulk regime at room temperature, this ADP technique has been applied to fabricate cathode layers and electrolyte films for lower temperature-operating solid oxide fuel cells (LT-SOFCs) as well as for the fabrication of an oxidation resistance coating layer on top of the metallic interconnectors in SOFCs [11,15,16].

In this work, the microstructural and electrochemical properties of an LSM/8YSZ composite cathode material prepared using the ADP technique without any subsequent high temperature treatment are investigated, especially for the use of this material in MS-SOFCs.

The developed ADP-LSM/8YSZ composite cathode was applied to a metal-supported cell and the electrochemical properties and thermal durability of this cell were investigated.

2. Experimental section

2.1. Sample preparation process using the ADP technique

The sample preparation procedure for ADP treated samples has been described in details elsewhere [11, 17]. The preparation procedures for composite cathodes via the application of the ADP technique are as follows: $La_{0.8}Sr_{0.2}MnO_{3-d}$ (LSM, Praxair) and 8 mol % yttria-stabilized zirconia (8YSZ, Tosoh) powders were used as the composite cathode materials and polyvinylidene fluoride (PVdF, Aldrich) was added as a pore former. To obtain an advanced triple phase boundary (TPB), the LSM powder was physically mixed with the 8YSZ powder for 6 h in a nylon jar ball mill using zirconia balls and ethanol as a solvent; this was followed by a drying step at 80 °C. The dried LSM-8YSZ-PVdF mixture was transported to a 25 x 0.8 mm^2 rectangular shaped nozzle through a tube with compressed air as carrier gas. The aerosol flow was accelerated by a rotary pump with a mechanical booster and a nozzle; aerosol was sprayed onto the dense 8YSZ electrolyte surface with high energy impact. The gap between the substrate and the nozzle was set to 5 mm. Following the ADP technique as described, the composite cathode system comprised of LSM-8YSZ was deposited on top of the dense 8YSZ electrolyte without heat treatment.

2.2. Sample preparation process for a symmetrical half cell

The cathodic polarizations displayed as Area Specific Resistance (ASR) were measured using symmetrical half cells. The 8YSZ electrolyte for the half cell measurement was fabricated using the powder compression technique; fabricated material was subsequently sintered at 1500 °C for 4 hours. This process produced a dense pellet (~95% of the calculated density) with a diameter of 26.0 mm and thickness of 1.5 mm.

In order to compare ASRs with respect to different fabrication processes such as ADP, screen printing and *in-situ* composite cathodes, symmetrical half cells were fabricated utilizing these different techniques. The term "*in-situ*" in this paper indicates that the coating process was carried out by screen printing and subsequent drying, but without additional heat treatment, so the cathodes prepared according to this method did not benefit from a sintering process.

For the ADP treated symmetrical half cell, the processes were carried out on 8YSZ electrolyte using the same experimental sequences as can be found in the literature [11, 17] with the experimental apparatus explained in chapter 2.1. In order to prepare the screen printed cathode, cathode inks for screen printing were fabricated using LSM (50 wt%)-8YSZ (50 wt%) with an acetone and a binder system comprised of α-terpineol and KD-1. These were coated onto the dense 8YSZ electrolytes using screen printing to fabricate the symmetrical half cells, which was sintered for 1 h at 1100 ^{o}C in order to form a porous electrode structure well bonded to the electrolyte. For the *in-situ* test cell, cathode layers were screen printed on both sides of the dense 8YSZ electrolyte and dried at 200^{o}C for 12 h without a subsequent sintering step. The final surface area of the symmetrical cell was about 1 cm^{2}.

2.3. Fabrication process of MS-SOFC

A fully sintered anode-supported ceramic cell consisting of NiO-8YSZ as the anode substrate and 8YSZ as the electrolyte, without a cathode layer was joined to a Stainless steel 430 (STS430, POSCO) metal support using a functional anode layer with a bonding property.

The functional anode layer used to connect the stainless steel with the anode supported SOFC single cell is composed of Ni-Cr-Fe powder (325-mesh, Alfa Aesar), 8YSZ, NiO (J.T. Baker) and graphite. STS430, with a plate thickness of 500 μm, was used as the metal support for the MS-SOFC application. The single serpentine channel required for the fuel gas

diffusion was fabricated by wire cutting [18, 19].

The functional anode layer was directly casted onto the metal support and sintered for 10 h at 1400 °C to promote adhesion between the interface of the metal part and the functional layer (anode supported SOFC cell without cathode layer). This step was carried out in a 4 % H_2/96 % Ar atmosphere to prevent the oxidation of the metal part. Afterwards the composite cathode was applied directly on top of the electrolyte using the ADP coating technique. The final cathode surface area and thickness were about 1 cm^2 and 12 μm. The thickness of anode-supported ceramic cell without cathode and metal support was 1mm. The MS-SOFC single cell fabricated in this way was used to measure the power density and impedance characteristics.

2.4. X-ray diffraction and microstructure analysis

X-ray diffraction (XRD) results were obtained in a RIGAKU D/MAX-IIIC (3 kW) using Cu Kα radiation (λ=0.15418 nm) operated under conditions of 40 kV and 45 mA. The data were collected at 0.06 ° steps with a counting time of 1 second per step, in the 2θ range from 20 ° to 80 °.

The microstructures of the symmetrical half cells were investigated using a field emission scanning electron microscope (FE-SEM, S-4200, Hitachi) combined with energy-dispersive spectroscopy (EDS).

2.5. Electrochemical characterization

Measurements of electrochemical properties and ASRs of the cathodes in air were conducted at open circuit voltage (OCV) as a function of temperature between 500 and 850 ^oC, with an increment of 50 ^oC. An AC four-probe method using a Solartron 1287/ Solartron 1260 (electrochemical interface impedance, gain-phase analyzer) was used to measure the electrochemical properties. The impedance measurements were conducted in a frequency

range of 5 MHz to 100 mHz; the amplitude of the applied voltage was 20 mV under OCV. The ASRs, measured from the differences between the first intercept in the vicinity of the high frequency and the last intercept at low frequency, were divided in two because the tested cells had two symmetrical electrodes.

Power densities were measured using the same Solatron with a four probe configuration. 3% H_2O humidified H_2 was supplied by bubbling H_2 fuel through de-ionized water to the anode chamber with a flow rate of 30 sccm. At the same time, compressed air was fed into the cathode side with a flow rate of 30 sccm.

3. Results and discussion

Figs. 1(a) and (b) show the X-ray diffraction (XRD) patterns of the $La_{0.8}Sr_{0.2}MnO_{3-d}$ (LSM) /8 mol % yttria-stabilized zirconia (8YSZ) composite cathode prepared using the aerosol deposition process (ADP) on a dense 8YSZ electrolyte at room temperature and of the LSM/8YSZ composite cathode sintered at 1100 °C after screen printing onto a dense 8YSZ electrolyte. In detail, in Fig. 1, open circles (○) and closed squares (■) respectively indicate peaks of the XRD patterns originating from LSM and 8YSZ. Each of the peaks observed in the XRD patterns can be assigned to either an LSM or to an 8YSZ single phase perovskite with stabilized cubic structure [20-22]. After the screen-printed sample is sintered at 1100 °C, no secondary phases or unknown phases are observed additional to the deposited LSM and the YSZ. Significantly, the broad peaks shown in Fig. 1(a) changed to sharp peaks after sintering in all ranges tested; comparing the XRD results of the sintered and the unsintered cathodes, this observation implies that the cathodes of the LSM/8YSZ prepared using ADP without heat treatment show relatively smaller particle sizes than do the cathodes prepared using heat treatment.

Figs. 2 and 3 show scanning electron microscopy (SEM) images of the ADP-LSM/8YSZ cathode and of the *in-situ* LSM/8YSZ composite cathode, both on a dense 8YSZ electrolyte.

The thickness of the deposited LSM/8YSZ layer fabricated with various coating techniques is approximately 12~14 μm. The cross-view images of the ADP-LSM/8YSZ and of the *in-situ* LSM/8YSZ composite cathode seem to show that these materials have similar structures, as can be seen in Fig. 2(a) and Fig. 3(a). However, when comparing the enlarged images that show the microstructural properties, as provided in Fig. 2(b) and Fig. 3(b), the sample using ADP treated LSM/8YSZ can be seen to have a melted surface shape and the *in-situ* sample shows the existence of randomly distributed LSM and 8YSZ phases, having various shapes and sizes without any certain tendency.

Top views of the two samples are provided in Fig. 2(c) and Fig. 3(c) under larger magnification. The grain boundaries and the interfaces between the particles of the ADP treated cathode can be distinctively seen in Fig. 2(c); in fact, they can be seen, much more clearly than those of the *in situ* cathode, which are shown in Fig. 3(c).

Fig. 4 provides a comparison of the cross-view microstructures of the ADP fabricated LSM/8YSZ composite cathode after sintering at 800 °C (Fig. 4(a)) and 1100 °C (Fig. 4(b)) and the *in-situ* treated LSM/8YSZ composite cathode sintered at 1100 °C. The compact structure of the sample shown in Fig. 2(a) changes to a porous microstructure after heat treatment, as shown in Fig. 4(a) and (b), because the PVdF organic material used in the ADP coating process was decomposed and then removed at 1100 °C. In addition, when increasing the heat treatment temperature from 800 ^{o}C to 1100 ^{o}C, the sintering effect of the composite cathodes comprised of LSM and 8YSZ was also measured; significantly, the relatively dense structure shown in Fig. 4(b), compared to that shown in Fig. 4(a), is believed to be caused by the sintering effect at high temperature. If the compact structure shown in Fig. 2(a) does not change, it can result in a lack of gas diffusion which would increase the cathodic polarization. However, no additional heat treatment step in the ADP composite cathodes is necessary because the porous structure automatically evolves at the elevated temperature of 800 °C during fuel cell operation.

When considering the differences in adhesion properties between the ADP-treated cathode shown in Fig. 2 and the sintered cathode shown in Fig. 4(c), the ADP-treated composite cathode shows better contact properties at the interface and the bulk. For example, the sintered sample was easily peeled off using 3M tape, but the sample prepared using the ADP technique showed stronger adhesion properties, proven by its getting stuck on 3M adhesive tape.

To compare the electrochemical properties with respect to the fabrication processes, Fig. 5 displays the impedance spectra of the symmetrical half cells measured at 700 °C. For example, Figs. 5(a) and (b) provided the impedance results for an ADP-LSM/8YSZ composite cathode fabricated at room temperature and an LSM/8YSZ composite cathode sintered at 1100 ^{o}C. In addition, Fig. 5(c) gives the impedance results for a half cell with an *in-situ* coated LSM/8YSZ cathode layer. The ASRs of the ADP-LSM/8YSZ sample shown in Fig. 5(a), the LSM/8YSZ sample sintered at 1100 °C shown in Fig. 5(b), and the *in-situ* treated LSM/8YSZ sample shown in Fig. 5(c) are approximately 1.50, 1.80, and 11.0 $\Omega \cdot cm^2$, respectively, at 700 ^{o}C. Comparing the results of the ADP treated sample shown in Fig. 5(a) and the *in-situ* sample shown in Fig. 5(c), the ADP-LSM/8YSZ sample shows a significantly lower ASR value than that of the sample prepared by the *in-situ* method, which is commonly used for conventional MS-SOFCs.

Considering the shape of the impedance arcs, the impedance plot of the *in-situ* treated LSM/8YSZ sample, shown in Fig. 5(c) appears to be a single merged circle, very similar to the shape of the impedance plot of the ADP-LSM/8YSZ sample shown in Fig. 5(a). An important result of the two impedance plots shown in Fig. 5(a) and (c) is that the plot of the ADP-treated sample consists of a single merged circle, which is different from the shape of the plot of the sintered sample, which shown in Fig. 5(b), and which displays two different arcs separated by a local minimum at a frequency of 1000Hz.

It is notable that, when considering the impedance arcs with respect to the frequency ranges, the high frequency resistance (R_H) associated with frequencies above 1000 Hz can be seen at the left side of the arc in the impedance plot of the ADP-LSM/YSZ half cell, but at the middle of the arc in the impedance plot of the half cell with the *in-situ* LSM/YSZ cathode fabricated without any sintering process after screen printing. The reason for this is that the interfacial state of the *in-situ* processed cathode is not connected to the electrolyte, rather, the cathode is deposited without any physical or chemical processes. According to the literature related to the behavior of impedance plots, the characteristic frequency of arcs in an impedance spectrum can give insight into the cathode reactions [23]. The resistance associated with high frequency (R_H) is generally related to charge transfer between particles. In particular, the resistance caused by charge transfer at the interface of an electrolyte and an electrode is presented as a high frequency (HF) semicircular region above 1000 Hz [23-26]. Considering this, the main differences between Figs. 5(a) and (c) can be explained as follows: the different positions of R_H in the arcs of the ADP-treated cathode in Fig. 5(a) and of R_H of the *in-situ* treated cathode in Fig. 5(c) are directly related to interfacial adhesion. The *in-situ* cathode with very poor interfacial properties suffers from a high ASR, which, due to the characteristic frequency of the related arc in the R_H range, can be related to interface contact problems. As can be seen in Fig. 2, the ADP-LSM/YSZ cathode shows highly enhanced interfacial adhesion between the cathode particles and between the cathode and the electrolyte. This advanced microstructure, caused by the high impact energy of ADP, obviously improved the electrochemical performance.

Fig. 6 shows summarized logarithmic ASR results for the ADP-LSM/8YSZ cathode layer without any sintering process as well as for the sintered LSM/8YSZ cathode layer prepared using screen printing; results are plotted against the inverse temperature. The ASRs of the ADP-treated sample are observed to be 1.50, 0.49 and 0.13 $\Omega \cdot cm^2$ at 700, 800, and 900 °C, respectively. The ASRs of the sintered samples are 1.12, 0.73, and 0.22 $\Omega \cdot cm^2$ at 700, 800,

and 900 °C, respectively. With respect to these measured results, it is important to note that the ADP sample shows smaller ASR values than those of the screen printed and sintered sample at measuring temperatures of 750 °C or higher. This indicates that the ADP technique can be directly applied to the cathode material of the MS-SOFC fabricated without a cathode sintering process because MS-SOFCs are generally operated at high temperature ranges (over 800 °C).

Fig. 7 provides a cross-sectional image of the anode in the developed MS-SOFC. The developed MS-SOFC consists of metal and ceramic parts in a layered formation of ADP-LSM/8YSZ composite cathode / 8YSZ electrolyte / 8YSZ-NiO anode (Anode layer 1) / Ni-Cr-Fe powder-8YSZ-NiO functional anode layer (Anode layer 2) / STS430 metal support. The electrode consist of an anode part comprised of NiO-8YSZ for the fuel oxidation, and a functional adhesive anode layer made of a Ni-Cr-Fe based powder, which connects the 8YSZ-NiO part to the STS metal support. The STS430 metal support layer, displayed at the bottom of Fig. 7, has 400 μm sized holes working as channels to allow gas diffusion.

Fig. 8(a) shows the current (I) - voltage (V) - power density (P) curve of an MS-SOFC with the ADP-LSM/8YSZ cathode at 800 °C. The open circuit voltage (OCV) value of the MS-SOFC cells comprised of the ADP-LSM / 8YSZ composite cathode / 8YSZ electrolyte / 8YSZ-NiO anode / Ni-Cr-Fe powder-8YSZ-NiO functional layer / STS metal support was found to be approximately 1.07 V, which is satisfactorily close to the theoretical value obtained from the Nernst equation [27]. Most importantly, the high OCV value indicates that the dense structure of the 8YSZ electrolyte has not been destroyed and is well formed by the many processing steps adopted in the fabrication of the MS-SOFCs. From the electrochemical properties shown in Fig. 8(a), the maximum power density of the ADP-LSM/8YSZ coated on an MS-SOFC is 0.38 $W \cdot cm^{-2}$ at 800 °C. Fig. 8(b) shows the long term stability of the ADP-LSM/8YSZ applied as a cathode material of an MS-SOFC. The cell performance is slightly degraded during the initial 12 h experiment time; this trend was found to continue until 30 h

after the start. The initial degradation of the cell may be caused by the created porous structure in the ADP-LSM/8YSZ cathode because the experimental temperature of 800 °C can affect the structure of the composite cathode shown in Fig. 4(a). Thereafter, the cell resistance does not significantly increase for the next 70 hours.

Fig. 8(c) shows the thermal cycling stability of the ADP-LSM/8YSZ coated MS-SOFC. Thermal cycling was conducted within the very severe temperature range between room temperature and 800 °C. The cycles numbered 1 to 6 in the legend in Fig. 8(c) show the number of thermal cycles. From these impedance plots, it can be seen that the ADP-LSM/8YSZ coated metal-supported cell shows nearly equivalent impedance results regardless of the thermal shock, except for slight increases in the low frequency ranges. Therefore, the MS-SOFC with ADP-LSM/8YSZ can be said to exhibit excellent thermal shock durability. These results derive from not only the robust metal-supported cell technology but also from the robust cathode-electrolyte system, with a perfectly joined interface following ADP.

4. Conclusions

LSM/8YSZ cathode formation without the use of a high temperature sintering process is an important requirement for MS-SOFCs with long-term stability and high cathode performance, because the oxidation of the metal component can be successfully avoided. The interfacial properties between the cathode and the electrolyte and between the particles of the cathode composite phases should be considered because they have a significant influence on the electrochemical behavior of the cell, even though good cathode performance is primarily related to the intrinsic electrocatalytic properties of the materials. The utilization of the ADP technique induces a strong interconnection between the particles and the layers via an anchoring effect induced by the high impact energy; this anchoring effect results in enhanced microstructural properties of ADP-LSM/8YSZ. The ADP-LSM/8YSZ cathode shows a low ASR values of approximately 1.50 $\Omega \cdot cm^2$ at 800 ^oC; the ADP-LSM/8YSZ coated MS-SOFC

shows a maximum power density of 0.38 $mW \cdot cm^{-2}$ at 800 °C. The stable performance of the MS-SOFC with ADP-LSM/8YSZ is confirmed through a severe thermal durability test.

Acknowledgements

The authors are grateful for the support of the Basic Science Research Program through the National Research Foundation of Korea (NRF), funded by the Ministry of Science, ICT & Future Planning (No. 2014R1A1A1004163), and from the academic research fund (2013) of Hanbat National University of South Korea.

References

[1] M. C. Tucker, G. Y. Lau, C. P. Jacobson, L. C. DeJonghe, S. J. Visco, Performance of metal-supported SOFCs with infiltrated electrodes, J. Power Sources 171 (2007) 477-482.

[2] S. Hui, D. Yang, Z. Wang, S. Yick, C. Decès-Petit, W. Qu, A. Tuck, R. Maric, D. Ghosh, Metal-supported solid oxide fuel cell operated at 400-600 °C, J. Power Sources 167 (2007) 336-339.

[3] Y. S. Xie, R. Neagu, C. S. Hsu, X. Zhang, C. Decès-Petit, Spray pyrolysis deposition of electrolyte and anode for metal-supported solid oxide fuel cell, J. Electrochem. Soc. 155 (2008) B407-B410.

[4] D. Waldbillig, O. Kesler, Characterization of metal-supported axial injection plasma sprayed solid oxide fuel cells with aqueous suspension plasma sprayed electrolyte layers, J. Power Sources 191 (2009) 320-329.

[5] C. Hwang, C. H. Tsai, C. H. Lo, C. H. Sun, Plasma sprayed metal supported YSZ/Ni–LSGM–LSCF ITSOFC with nanostructured anode, J. Power Sources 180 (2008) 132-142.

[6] Y. Zhao, C. Xia, L. Jia, Z. Wang, H. Li, J. Yu, Y. Li, Recent progress on solid oxide fuel cell: Lowering temperature and utilizing non-hydrogen fuels, Int. J. Hydrogen Energy 38 (2013) 16498-16517.

[7] Y. M. Kim, P. Kim-Lohsoontorn, J. Bae, Effect of unsintered gadolinium-doped ceria buffer layer on performance of metal-supported solid oxide fuel cells using unsintered barium strontium cobalt ferrite cathode, J. Power Sources 195 (2010) 6420-6427.

[8] Y. Zhou, X. Xin, J. Li, X. Ye, C. Xia, S. Wang, Z. Zhan, Performance and degradation of metal-supported solid oxide fuel cells with impregnated electrodes, Int. J. Hydrogen Energy 39 (2014) 2279-2285.

[9] Y. Kong, B. Hua, J. Pu, B. Chi, L. Jian, A cost-effective process for fabrication of metal-supported solid oxide fuel cells, Int. J. Hydrogen Energy 35 (2010) 4592-4596.

[10] J. Choi, T. Lee , M. Choi, Y. S. Yoo, S. W. Baek, J. Bae, Long-term performance of anode-supported SOFC integrated with metal interconnect by joining process, Int. J. Hydrogen Energy 35 (2010) 4285-4291.

[11] J. J. Choi, S.H. Oh, H. S. Noh, H. R. Kim, J. W. Son, D. S. Park, J.H. Choi, J. Ryu, B. D. Hahn, W. H. Yoon, H. W. Lee, Low temperature fabrication of nano-structured porous LSM-YSZ composite cathode film by aerosol deposition, J. Alloys Comp. 509 (2011) 2627-2630.

[12] D. Stöver, D. Hathiramani, R. Vaßen, R. J. Damani, Plasma-sprayed components for SOFC applications, Surf. Coat. Technol. 201 (2006) 2002-2005.

[13] I. Villareal, C. P. Jacobson, A. Leming, Y. Matus, S. J. Visco, L.C.D. Jonghe, Metal-supported solid oxide fuel cells, Electrochem. Solid-State Lett. 6 (2003) A178-A179.

[14] M. Lang, T. Franco, R. Henne, S. Schaper, G. Schiller, Characterization of vacuum plasma sprayed thin film SOFC for reduced operating temperatures, Proc. the 4th European Solid Oxide Fuel Cell Forum 106 (2000) 231-240.

[15] J. J. Choi, K.S. Cho, J.H. Choi, J. Ryu, B.D. Hahn, W.H. Yoon, J.W. Kim, C.W. Ahn, J. Yun, D.S. Park, Low temperature preparation and characterization of LSGMC based IT-SOFC cell by aerosol deposition, J. Eur. Ceram. Soc. 32 (2012) 115-121.

[16] J.J. Choi, K.S. Cho, J.H. Choi, J. Ryu, B.D. Hahn, J.W. Kim, C.W. Ahn, W.H. Yoon, J. Yun, D.S. Park, Effects of annealing temperature on solid oxide fuel cells containing (La,Sr)(Ga,Mg,Co)$O_{3-\delta}$ electrolyte prepared by aerosol deposition, Mater. Lett. 70 (2012) 44-47

[17] J. J. Choi, B. D. Hahn, J. Ryu, W. H. Yoon, D.S. Park, ''Effects of $Pb(Zn_{1/3}Nb_{2/3})O_3$ addition and post-annealing temperature on the electrical properties of $Pb(Zr_xTi_{1-x})O_3$ thick films prepared by aerosol deposition method, J. Appl. Phys. 102 (2007) 044101(1)-044101(6).

[18] S. W. Baek, J. Jeong, J. H. Kim, C. Lee, J. Bae, Interconnect-integrated solid oxide fuel cell with high temperature sinter-joining process, Interconnect-integrated solid oxide fuel cell with high temperature sinter-joining process, Int. J. Hydrogen Energy 35 (2010) 11878-11889.

[19] J. Park, Y. M. Kim, J. Bae, A numerical study on the heat and mass transfer characteristics of metal-supported solid oxide fuel cells, Int. J. Hydrogen Energy 36 (2011) 3167-3178.

[20] D. Grossin, J. G. Noudem, Synthesis of fine $La_{0.8}Sr_{0.2}MnO_3$ powder by different ways, Solid State Sci. 6 (2004) 939-944.

[21] V. S. Reddy Channu, R. Holze, E. H. Walker, Synthesis and characterization of $La_{0.8}Sr_{0.2}MnO_{3-\delta}$ nanostructures for solid oxide fuel cells, New J. Glass and Ceramics, 3 (2013) 29-33.

[22] C. W. Kuoa, Y. H. Shena, I. M. Hung, S. B. Wenc, H. E. Lee, M. C. Wang, Effect of Y_2O_3 addition on the crystal growth and sintering behavior of YSZ nanopowders prepared by a sol-gel process, J. Alloys Comp. 472 (2009) 186-193.

[23] S. W. Baek, J. Bae, Y. S. Yoo, Cathode reaction mechanism of porous-structured $Sm_{0.5}Sr_{0.5}CoO_{3-\delta}$ and $Sm_{0.5}Sr_{0.5}CoO_{3-\delta}$ / $Sm_{0.2}Ce_{0.8}O_{1.9}$ for solid oxide fuel cells, J. Power Sources 193 (2009) 431-440.

[24] S.B. Adler, Factors governing oxygen reduction in solid oxide fuel cell cathodes, Chem. Rev. 104 (2004) 4791-4843.

[25] S. W. Baek, J. H. Kim, J. Bae, Characteristics of ABO_3 and A_2BO_4 (A=Sm, Sr ; B=Co, Fe, Ni) samarium oxide system as cathode materials for intermediate temperature-operating solid oxide fuel cell, Solid State Ion. 179 (2008) 1570-1574.

[26] E. Perry Murray, M. J. Sever, S. A. Barnett, Electrochemical performance of $(La,Sr)(Co,Fe)O_3$–$(Ce,Gd)O_3$ composite cathodes, Solid State Ion. 148 (2002) 27-34.

[27] B. Wei, Z. Lü, S. Li, Y. Liu, K. Liu, W. Su, Thermal and electrical properties of new cathode material $Ba_{0.5}Sr_{0.5}Co_{0.8}Fe_{0.2}O_{3-\delta}$ for solid oxide fuel cells, Electrochem. Solid State Lett. 8 (2005) A428-A431.

Figure captions

Fig. 1. XRD diagrams of (a) LSM/8YSZ fabricated by aerosol deposition at room temperature and (b) LSM/8YSZ fabricated by screen printing and subsequent sintering at 1100 ^{o}C.

Fig. 2. SEM images of an ADP-LSM/8YSZ composite cathode on a dense 8YSZ electrolyte showing (a) a cross-section image, (b) an enlarged cross-section image, and (c) a top-view image.

Fig. 3. SEM images of an *in-situ* LSM/8YSZ composite cathode on a dense 8YSZ electrolyte showing (a) a cross-section image, (b) an enlarged cross-section image, and (c) a top-view image.

Fig. 4. SEM images of (a) ADP-LSM/8YSZ composite cathode sintered at 800 ^{o}C, (b) ADP-LSM/8YSZ composite cathode sintered at 1100 ^{o}C, and (c) *in-situ* LSM/8YSZ composite cathode sintered at 1100 ^{o}C.

Fig. 5. Impedance spectra of half cells fabricated using different processes: (a) ADP-LSM/8YSZ, (b) screen printed LSM/8YSZ sintered at 1100 ^{o}C, and (c) *in-situ* LSM/8YSZ cathode without heat treatment.

Fig. 6. Arrhenius plot of area specific resistances (ASRs) of the ADP-LSM/8YSZ composite cathode without sintering process and of the sintered LSM/8YSZ composite cathode.

Fig. 7. Structure of the developed metal-supported cell; Anode layer 1: 8YSZ-NiO anode, Anode layer 2: Ni-Cr-Fe powder-8YSZ-NiO functional anode.

Fig. 8. (a) Current (I) - voltage (V) - power density (P) curve of the ADP-LSM/8YSZ coated metal-supported cell measured at 800 ^{o}C, (b) impedance spectra (long term stability) of ADP-LSM/8YSZ coated metal-supported cell measured at 800 ^{o}C, and (c) impedance spectra (thermal cycles) of the ADP-LSM/8YSZ coated metal-supported cell between 800 ^{o}C and room temperature.

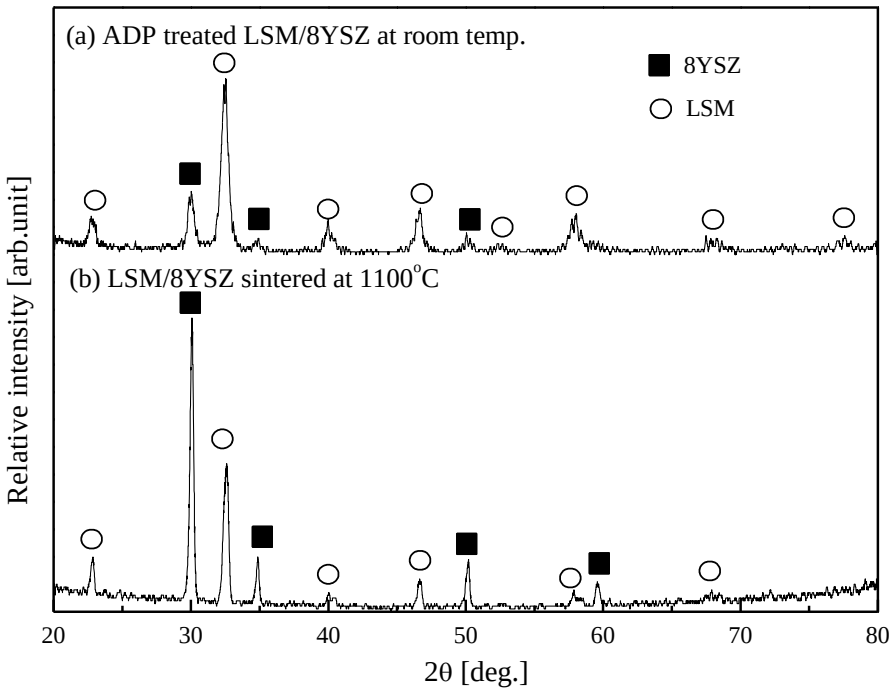

Fig. 1. XRD diagrams of (a) LSM/8YSZ fabricated by aerosol deposition at room temperature and (b) LSM/8YSZ fabricated by screen printing and subsequent sintering at 1100 °C.

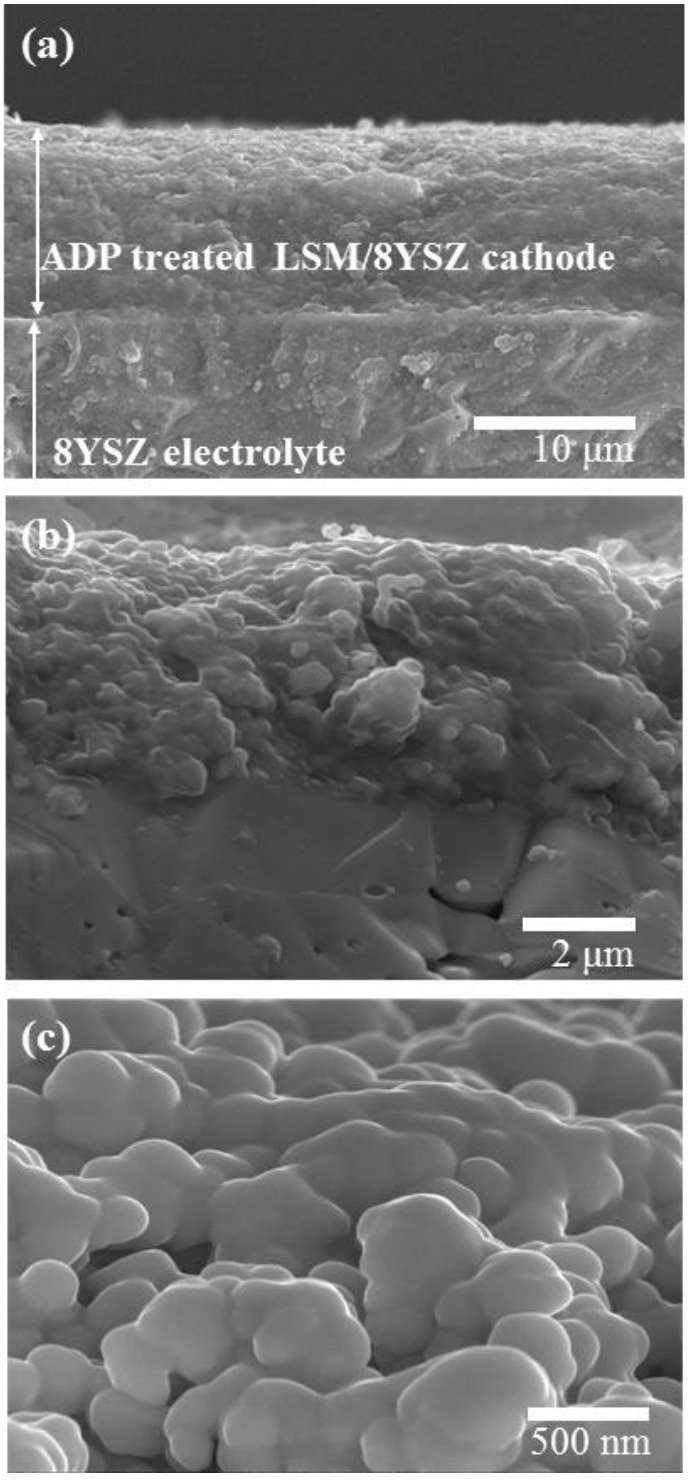

Fig. 2. SEM images of an ADP-LSM/8YSZ composite cathode on a dense 8YSZ electrolyte showing (a) a cross-section image, (b) an enlarged cross-section image, and (c) a top-view image.

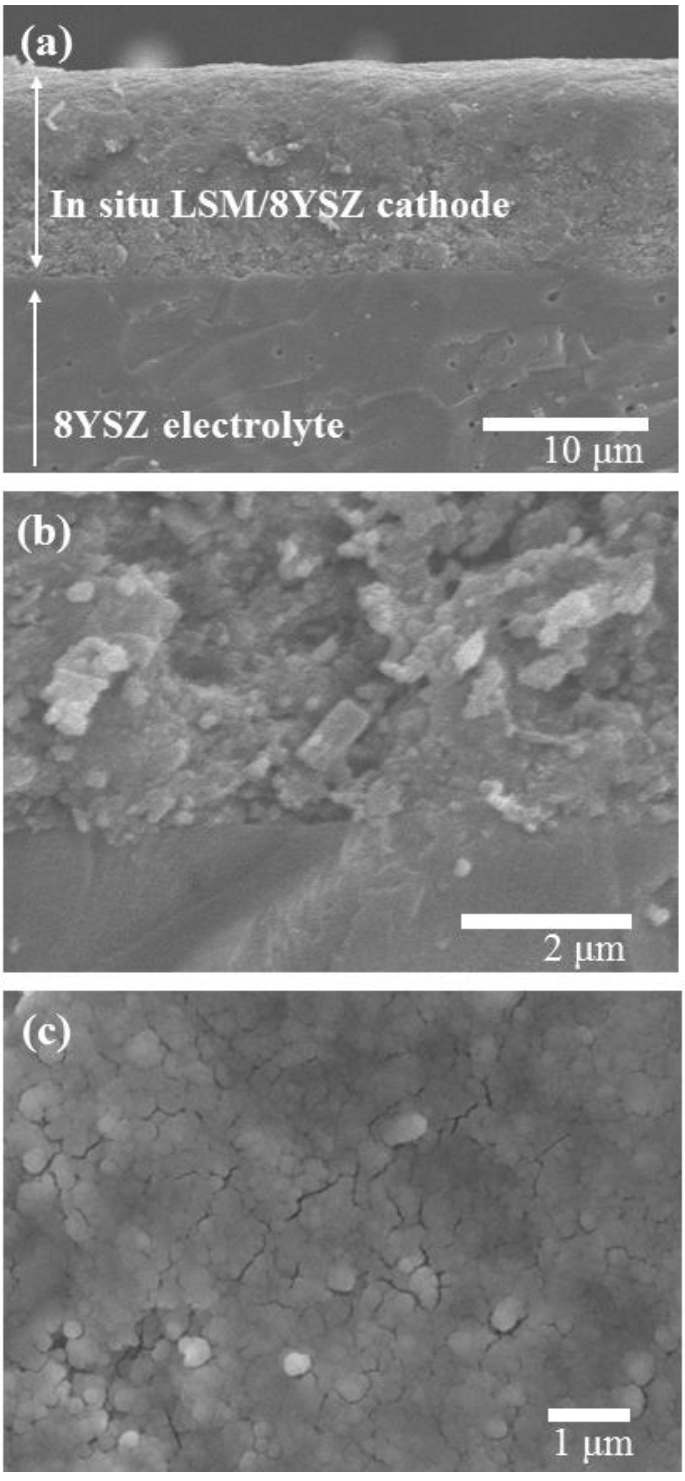

Fig. 3. SEM images of an *in-situ* LSM/8YSZ composite cathode on a dense 8YSZ electrolyte showing (a) a cross-section image, (b) an enlarged cross-section image, and (c) a top-view image.

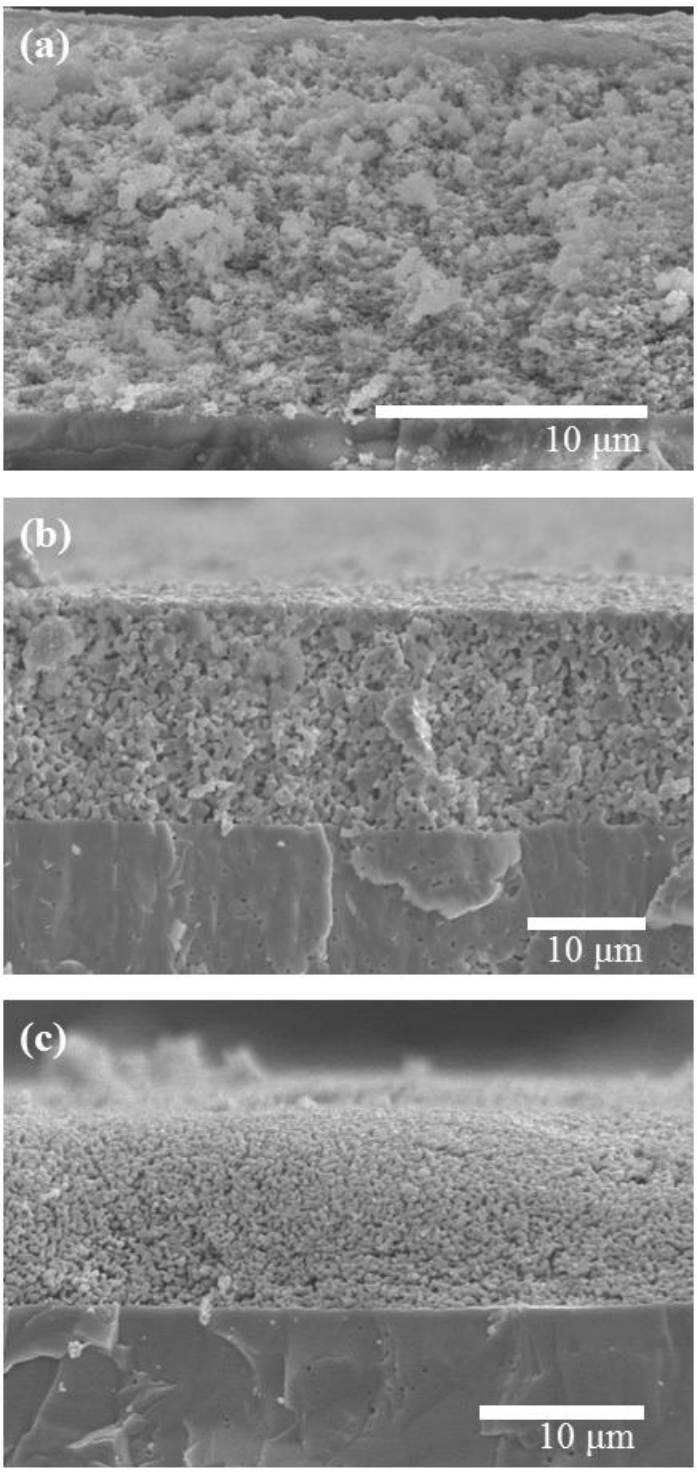

Fig. 4. SEM images of (a) ADP-LSM/8YSZ composite cathode sintered at 800 ^{o}C, (b) ADP-LSM/8YSZ composite cathode sintered at 1100 ^{o}C, and (c) *in-situ* LSM/8YSZ composite cathode sintered at 1100 ^{o}C.

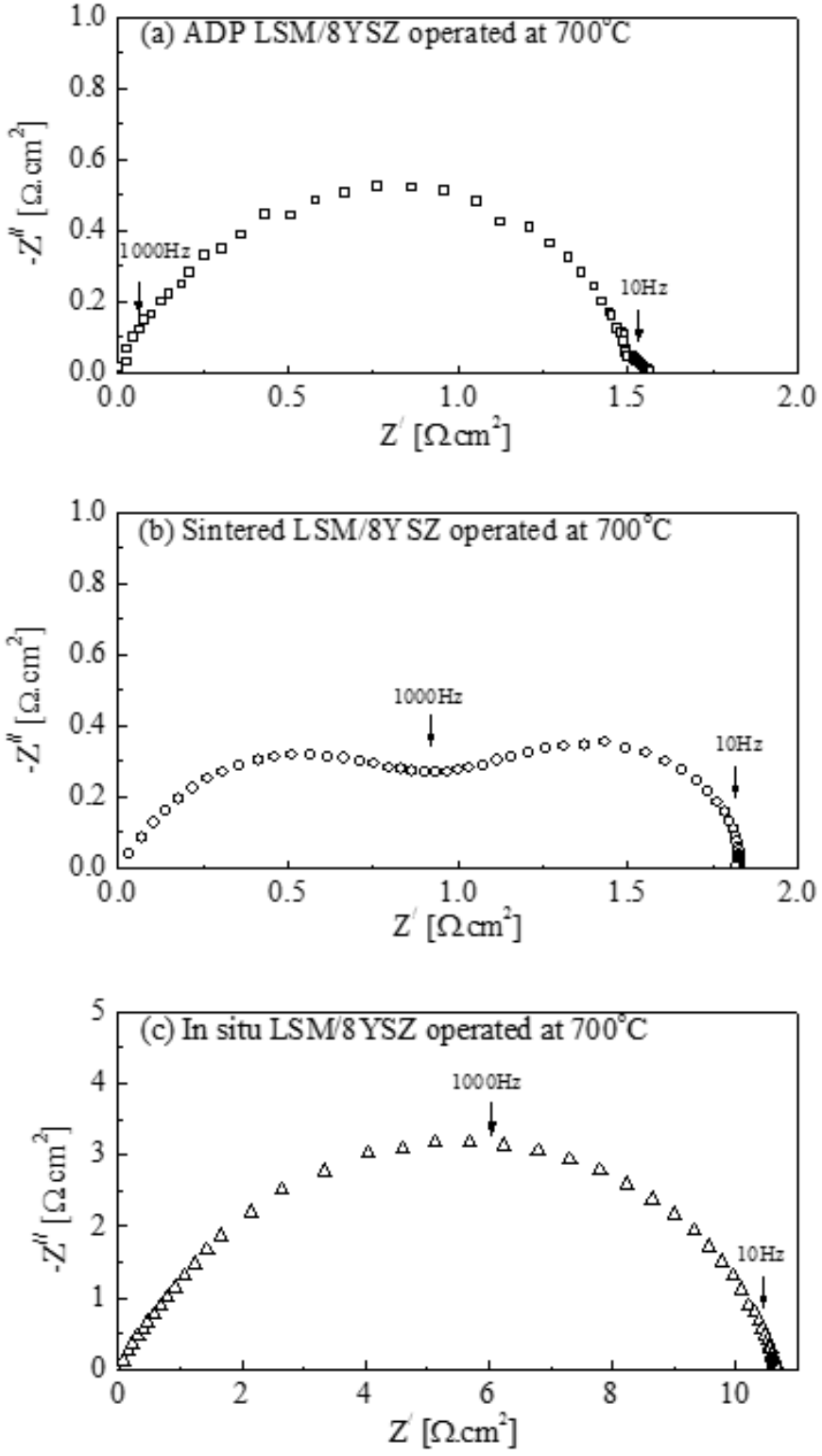

Fig. 5. Impedance spectra of half cells fabricated using different processes: (a) ADP-LSM/8YSZ, (b) screen printed LSM/8YSZ sintered at 1100 °C, and (c) *in-situ* LSM/8YSZ cathode without heat treatment.

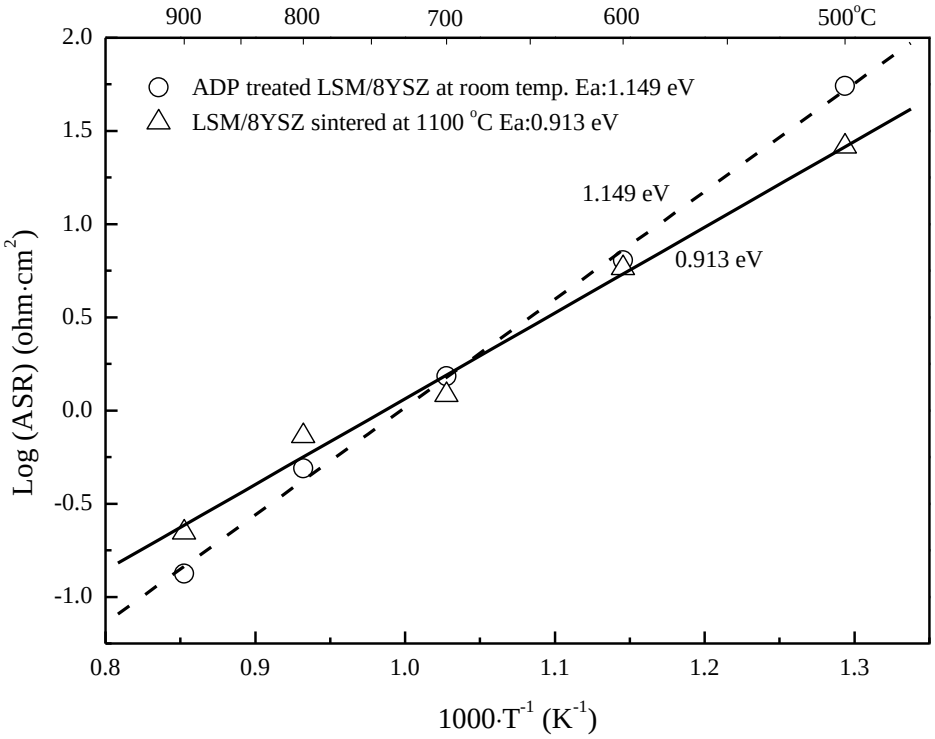

Fig. 6. Arrhenius plot of area specific resistances (ASRs) of the ADP-LSM/8YSZ composite cathode without sintering process and of the sintered LSM/8YSZ composite cathode.

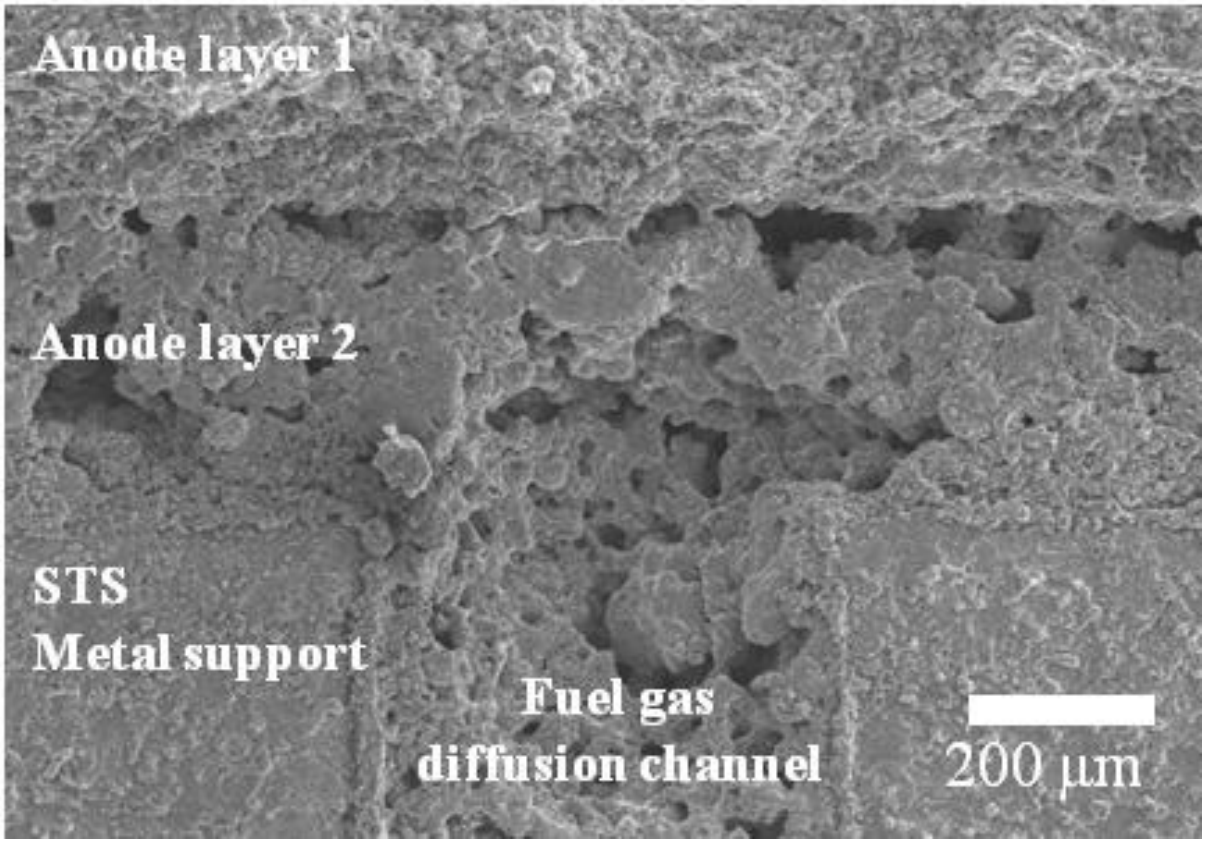

Fig. 7. Structure of the developed metal-supported cell; Anode layer 1: 8YSZ-NiO anode, Anode layer 2: Ni-Cr-Fe powder-8YSZ-NiO functional anode.

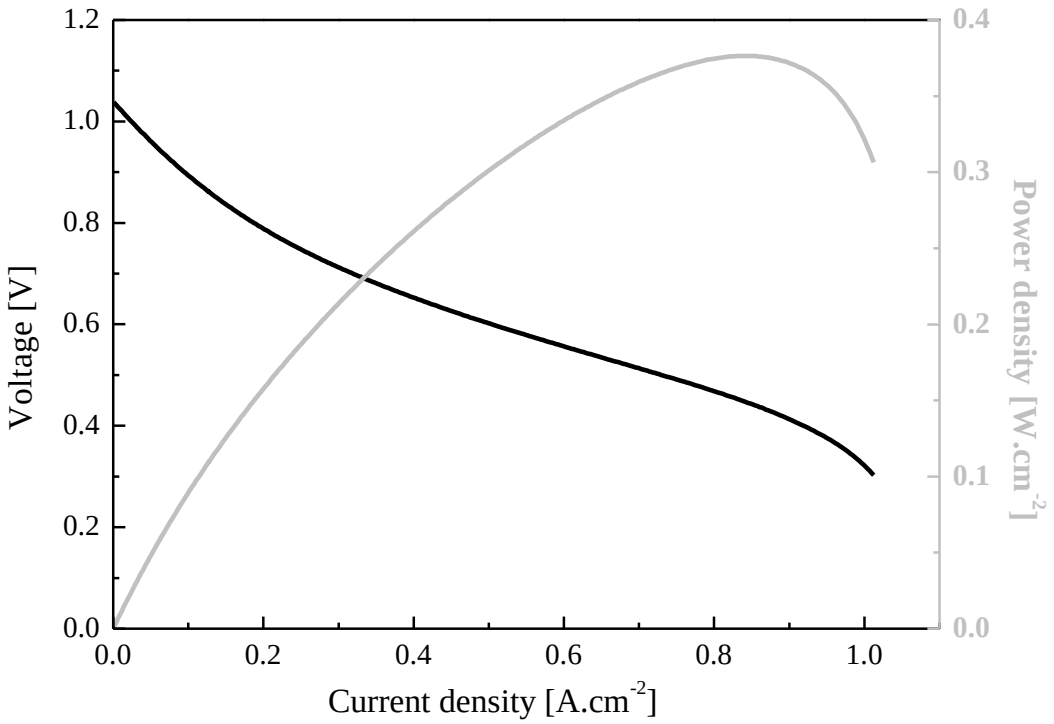
Voltage [V]
Power density [W.cm-2]
Current density [A.cm-2]
0.0
0.2
0.4
0.6
0.8
1.0
1.2
0.1
0.3

Fig. 8. (a)

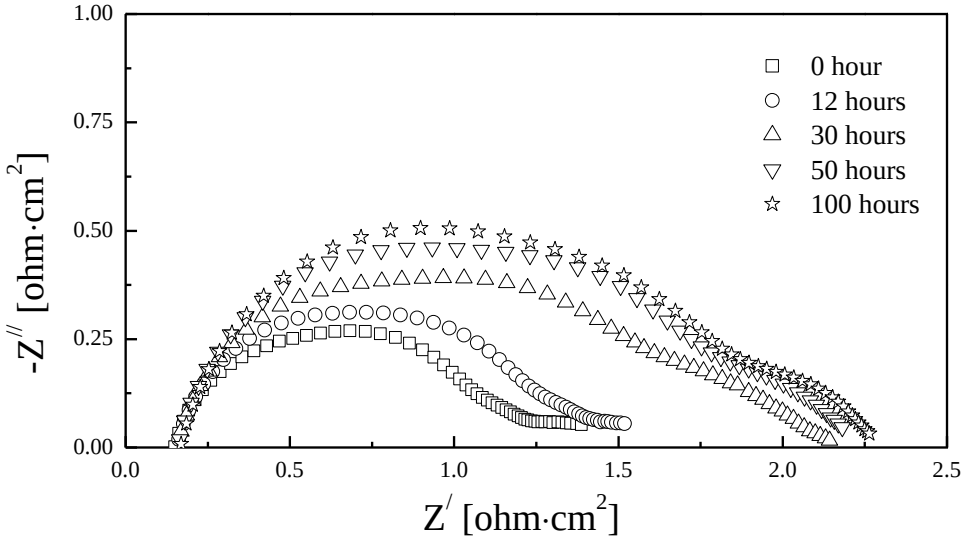
1.00
0.75
0.50
0.25
0.00
0.0
0.5
1.0
1.5
2.0
2.5
-Z'' [ohm·cm2]
Z' [ohm·cm2]
0 hour
12 hours
30 hours
50 hours
100 hours

Fig. 8. (b)

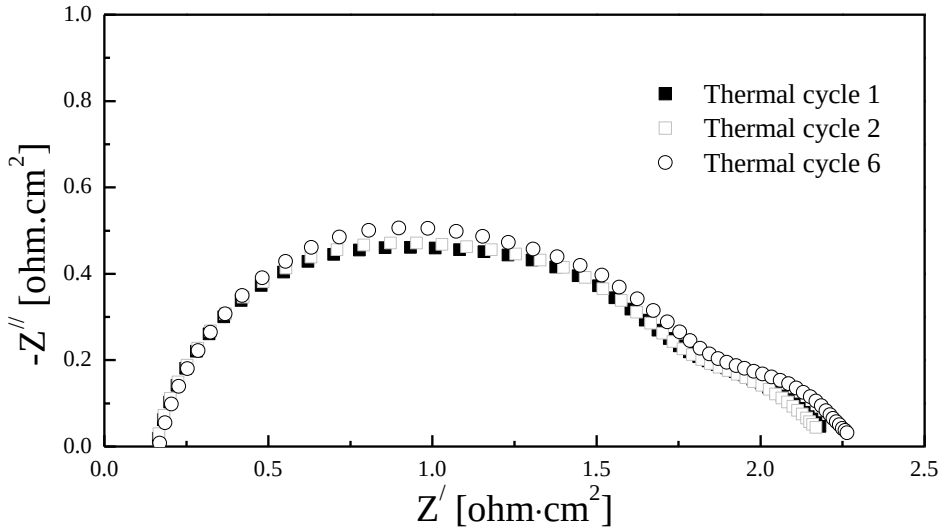

Fig. 8. (c)

Fig. 8. (a) Current (I) - voltage (V) - power density (P) curve of the ADP-LSM/8YSZ coated metal-supported cell measured at 800 ^{o}C, (b) impedance spectra (long term stability) of ADP-LSM/8YSZ coated metal-supported cell measured at 800 ^{o}C, and (c) impedance spectra (thermal cycles) of the ADP-LSM/8YSZ coated metal-supported cell between 800 ^{o}C and room temperature.